Dalton Transactions

PAPER

View Article Online
View Journal | View Issue

Cite this: *Dalton Trans.*, 2014, **43**, 14959

Structural and thermodynamic similarities of phases in the Li–Tt (Tt = Si, Ge) systems: redetermination of the lithium-rich side of the Li–Ge phase diagram and crystal structures of $Li_{17}Si_{4.0-x}Ge_x$ for x = 2.3, 3.1, 3.5, and 4 as well as $Li_{4.1}Ge$†

Michael Zeilinger and Thomas F. Fässler*

Received 12th March 2014,
Accepted 12th May 2014

DOI: 10.1039/c4dt00743c

www.rsc.org/dalton

A reinvestigation of the lithium-rich section of the Li–Ge phase diagram reveals the existence of two new phases, $Li_{17}Ge_4$ and $Li_{4.10}Ge$ ($Li_{16.38}Ge_4$). Their structures are determined by X-ray diffraction experiments of large single crystals obtained from equilibrated melts with compositions $Li_{95}Ge_5$ and $Li_{85}Ge_{15}$. Excess melt is subsequently removed through isothermal centrifugation at 400 °C and 530 °C, respectively. $Li_{17}Ge_4$ crystallizes in the space group $F\bar{4}3m$ (a = 18.8521(3) Å, V = 6700.1(2) Å^3, Z = 20, T = 298 K) and $Li_{4.10}Ge$ ($Li_{16.38}Ge_4$) in $Cmcm$ (a = 4.5511(2) Å, b = 22.0862(7) Å, c = 13.2751(4) Å, V = 1334.37(8) Å^3, Z = 16, T = 123 K). Both phases are isotypic with their Si counterparts and are further representative of the $Li_{17}Pb_4$ and $Li_{4.11}Si$ structure types. Additionally, the solid solutions $Li_{17}Si_{4-x}Ge_x$ follows Vegard's law. A comparison of the $GeLi_n$ coordination polyhedra shows that isolated Ge atoms are 13- and 14-coordinated in $Li_{17}Ge_4$, whereas in $Li_{16.38}Ge_4$ the Ge atoms possess coordination numbers 12 and 13. Regarding the thermodynamic stability, $Li_{16.38}Ge_4$ is assigned a high-temperature phase existing between ~400 °C and 627 °C, whereas $Li_{17}Ge_4$ decomposes peritectically at 520–522 °C. Additionally, the decomposition of $Li_{16.38}Ge_4$ below ~400 °C was found to be very sluggish. These findings are manifested by differential scanning calorimetry, long-term annealing experiments and the results from melt equilibration experiments. Interestingly, the thermodynamic properties of the lithium-rich tetrelides $Li_{17}Tt_4$ and $Li_{4.1}Tt$ ($Li_{16.4}Tt_4$) are very similar (Tt = Si, Ge). Besides $Li_{15}Tt_4$, $Li_{14}Tt_6$, $Li_{12}Tt_7$, and LiTt, the title compounds are further examples of isotypic tetrelides in the systems Li–Tt.

Introduction

In the last decade, the demand for high capacity lithium-ion batteries (LIBs) decisively influenced numerous fields of research; in particular, the chemistry of group 14 elements (tetrel = Tt) plays an important role in the development of more efficient anode materials. Since Si theoretically offers a specific capacity of 3579 mA h g^{-1} (based on the formation of $Li_{15}Si_4$) and thus massively exceeds the capacity of the commonly used graphite anode (372 mA h g^{-1}, LiC_6),[1,2] research on Li–Si materials has been in focus for many years. As the high capacity of Si is associated with several problems such as a large volume expansion of up to 300% upon lithiation accompanied by contact loss of electrodes and poor cycle life, a large number of these studies target these issues.[3] Further, Li–Si phases predominantly occur amorphously during charging and discharging, and only at low discharge voltages, crystalline $Li_{15}Si_4$ is observed.[1,2,4,5] However, the processes in working LIBs can be nicely monitored by *in situ*/*ex situ* NMR investigations.[6,7] Moreover, a fundamental understanding of thermodynamic properties and an unambiguous structural characterization of Li–Si phases are of considerable impor-

Department Chemie, Technische Universität München, Lichtenbergstraße 4, 85747 Garching b. München, Germany. E-mail: Thomas.Faessler@lrz.tum.de, michael.zeilinger@mytum.de; Tel: (+49) 89 289 13131

†Electronic supplementary information (ESI) available: Crystallographic data, refinement results, fractional atomic coordinates, and isotropic equivalent atomic displacement parameters for $Li_{17}Si_{4-x}Ge_x$ [x = 2.30(2), 3.08(4), 3.53(3)] (Table S1–4), comparison of experimental and computational relaxed fractional atomic coordinates for both $Li_{21}Si_5$ and $Li_{17}Si_4$ (Table S5), experimental fractional atomic coordinates for $Li_{17}Si_4$, $Li_{17}Ge_4$, $Li_{17-\varepsilon}Zn_\varepsilon Ge_4$, and $Li_{16.95}Ge_4$ (Table S6), comparison of experimental fractional atomic coordinates for $Li_{16.95}Ge_4$ and computational relaxed ones for $Li_{21}Si_5$ (Table S7), PXRD patterns of "$Li_{16}Ge_4$" samples annealed at various temperatures (Fig. S1), Rietveld refinement results for $Li_{17}Si_{4-x}Ge_x$ (x = 0, 2.30(2), 3.08(4), 3.53(3), 4) (Fig. S2). See DOI: 10.1039/c4dt00743c

tance. Just recently, we reported on detailed investigations on lithium-rich silicides, including the metastable phase $Li_{15}Si_4$,[8] $Li_{17}Si_4$[9] and the high-temperature phase $Li_{4.11}Si$ ($Li_{16.42}Si_4$).[10] Further examples are given in ref. 11–17.

The heavier tetrel element Ge has received less attention regarding its use as an anode material due to its low natural abundance connected with a lower theoretical specific capacity compared to silicon (1564 mA h g^{-1} *vs.* 4056 mA h g^{-1}, based on the formation of $Li_{16.95}Ge_4$[18] and $Li_{17}Si_4$,[9] respectively). However, the diffusivity of lithium in Ge is approximately 400 times larger than in Si at room temperature,[19,20] which intrinsically puts germanium to the foreground. Since some Si analogues are not known we put emphasis on the structural variety of lithium germanides and their thermodynamic relation.

Li–Ge phases were first postulated in the 1950s and 1960s (Li_3Ge, Li_4Ge, LiGe),[21–23] fueling numerous investigations in this field later on. Before 2001, the ascertained Li–Ge representatives included $Li_{21}Ge_5$[24] (formerly described as $Li_{20}Ge_5$[25,26] and $Li_{22}Ge_5$[27,28]), $Li_{15}Ge_4$,[28,29] $Li_{13}Ge_4$[30] (formerly reported as Li_7Ge_2[31]), $Li_{14}Ge_6$,[25,26] Li_9Ge_4,[32] $Li_{12}Ge_7$,[25,26,33] LiGe (space group $I4_1/a$, ambient pressure),[22,34] LiGe (space group $I4_1/amd$, high pressure),[35] and Li_7Ge_{12}.[26,36] A previously described phase $Li_{11}Ge_6$[37] could not be reproduced in the course of the redetermination of the Li–Ge phase diagram by Grüttner,[25] and due to the "striking similarity" to Li_8MgSi_6,[38] it might have been ternary Li_8MgGe_6. Until then, solely $Li_{21}Tt_5$, $Li_{14}Tt_6$, $Li_{12}Tt_7$, and LiTt (LiSi[39] is obtainable from high-pressure synthesis) were known for both Si and Ge. We note that $Li_{13}Si_4$ and $Li_{13}Ge_4$ are not isotypic and crystallize with their own structure types. In the following years new Li–Tt phases were found and others were revised, *e.g.* a hexagonal high-pressure form of LiGe (space group $P6_3/mmc$),[40] metastable $Li_{15}Si_4$[1,2] being isotypic with the congruently melting phase $Li_{15}Ge_4$[25] ($Li_{15}Tt_4$), $Li_{\sim 17}Ge_4$ ($Li_{21+3/16}Si_5$ = $Li_{16.95}Ge_4$)[18] revised from $Li_{21}Ge_5$, and the revision of the Li_7Ge_{12} structure.[41] The synthesis of solid solutions $Li_{15}Si_{4-x}Ge_x$ by mechanical ball-milling was also reported.[42] An experimental determination of the Li–Ge phase diagram involving most of the aforementioned phases is given by Grüttner in his dissertation.[25]

We recently reported on the single crystal structures and thermodynamic properties of $Li_{17}Si_4$,[9] the high-temperature phase $Li_{4.11}Si$ ($Li_{16.42}Si_4$),[10] and metastable $Li_{15}Si_4$.[8] The Li–Si phase diagram was revised accordingly. Consequently, we extended our studies on the Li–Ge system. Herein, we present the single crystal X-ray structure determination of $Li_{17}Ge_4$ and $Li_{4.10}Ge$ which crystallize isotypically with their Si counterparts. Earlier structure reports on $Li_{\sim 17}Ge_4$ ($Li_{21+3/16}Si_5$ = $Li_{16.95}Ge_4$)[18] involving partially occupied Li sites could not be confirmed. Solid solutions of the isotypic phases $Li_{17}Si_4$ and $Li_{17}Ge_4$ follow Vegard's law.[43] Due to clarity and a better comparability, the phase $Li_{4.10}Ge$ is referred to as $Li_{16.38}Ge_4$. Furthermore, the lithium-rich section of the Li–Ge phase diagram (Li concentrations >79 at%) is reinvestigated by differential scanning calorimetry and long-term annealing experiments, manifesting $Li_{16.38}Ge_4$ as a high-temperature phase which possesses a very sluggish decomposition behavior below ~400 °C. $Li_{17}Ge_4$ is peritectically formed at 520–522 °C from cooling an according melt.

Results and discussion

Single crystal X-ray structure determination of $Li_{17}Ge_4$ and $Li_{16.38}Ge_4$

Large single crystals of $Li_{17}Ge_4$ and $Li_{16.38}Ge_4$ were grown in Li–Ge melts $Li_{95}Ge_5$ and $Li_{85}Ge_{15}$ at 400 °C and 530 °C, respectively. For $Li_{16.38}Ge_4$, bar-shaped crystals with a size of up to 0.6 × 0.25 × 0.25 cm^3 could be obtained. A representative specimen is depicted in Fig. 1. Generally, crystals of $Li_{17}Ge_4$ grew much smaller in a block-like shape with diameters of 0.1 × 0.1 × 0.1 cm^3. Those crystals allowed acquisition of high quality single crystal X-ray diffraction data.

The phase $Li_{17}Ge_4$ crystallizes in the space group $F\bar{4}3m$ with a = 18.8521(3) Å (V = 6700.1(2) $Å^3$) and Z = 20. The asymmetric unit consists of 13 Li and four Ge atoms each being located on a special position (Table 1). As already reported for $Li_{17}Si_4$, $Li_{17}Sn_4$, and $Li_{17}Pb_4$,[9,18,44] the Wyckoff position 4*a* with symmetry $\bar{4}3m$ was found to be fully occupied. We note that the refinement of occupancy factors did not indicate significantly large deviations from full occupancy and thus they were regarded as being fully occupied. Accordingly, the cubic unit cell of $Li_{17}Ge_4$ contains 340 Li and 80 Ge atoms ($cF420$). Further, atomic displacement parameters were refined anisotropically with meaningful results for all atoms, revealing excellent reliability factors of R_1 = 0.022 and wR_2 = 0.038 (all data) for the final model (Table 6). The structure of $Li_{17}Ge_4$ is isotypic with $Li_{17}Si_4$, $Li_{17}Sn_4$, and $Li_{17}Pb_4$.[9,18,44]

$Li_{16.38(2)}Ge_4$ crystallizes in the space group $Cmcm$ with a = 4.5511(2) Å, b = 22.0862(7) Å, c = 13.2751(4) Å (V = 1334.37(8) $Å^3$) and Z = 16 referring to $Li_{4.096(4)}Ge$ as one formula unit. The

Fig. 1 Example of a bar-shaped single crystal of $Li_{16.38}Ge_4$ obtained from a melt $Li_{85}Ge_{15}$ at 530 °C.

Table 1 Fractional atomic coordinates and isotropic equivalent atomic displacement parameters for $Li_{17}Ge_4$ ($F\bar{4}3m$, Z = 20, T = 298 K, estimated standard deviations in parentheses)

Atom	Wyckoff position	x	y	z	U_{eq}/Å^2·10^3
Ge1	16*e*	0.159545(8)	*x*	*x*	13.03(4)
Ge2	16*e*	0.916568(8)	*x*	*x*	11.37(4)
Ge3	24*f*	0.32102(1)	0	0	13.27(5)
Ge4	24*g*	0.57015(1)	1/4	1/4	13.06(4)
Li1	16*e*	0.0734(2)	*x*	*x*	31(1)
Li2	16*e*	0.3031(2)	*x*	*x*	21.6(8)
Li3	16*e*	0.4175(2)	*x*	*x*	22.3(9)
Li4	16*e*	0.5575(2)	*x*	*x*	23(1)
Li5	16*e*	0.6877(2)	*x*	*x*	28(1)
Li6	16*e*	0.8314(2)	*x*	*x*	27(1)
Li7	24*f*	0.1677(3)	0	0	25(1)
Li8	24*g*	0.0743(3)	1/4	1/4	23.1(9)
Li9	48*h*	0.0913(2)	*x*	0.2624(2)	32.0(9)
Li10	48*h*	0.0896(2)	*x*	0.7612(2)	31.1(8)
Li11	48*h*	0.1547(1)	*x*	0.5205(2)	32.5(8)
Li12	48*h*	0.1637(1)	*x*	0.0027(2)	22.5(8)
Li13	4*a*	0	0	0	17(2)

unit cell contains 10 Li and three Ge atom positions (Table 2) where Li4 and Li5 are disordered. A careful analysis of difference Fourier maps after assigning all Ge and nine Li atom positions (Li1–Li3 and Li5–Li10) revealed occupational disorder along the crystallographic *a*-axis like that reported for $Li_{16.42}Si_4$.[10] As can be seen in Fig. 2a and 2b, the difference Fourier maps showing the strand-like residual electron density with peak-maxima at Wyckoff positions 4*c* and 8*g* are almost identical for $Li_{16.42(1)}Si_4$ and $Li_{16.38(2)}Ge_4$. Applying the disorder model as reported for $Li_{16.42(1)}Si_4$,[10] we subsequently obtained a very similar occupancy ratio of 0.616(8)/0.384(8) for Li4A on 4*c* (1/2, *y*, 1/4) and Li4B on 8*g* (*x*, *y*, 1/4), respectively, compared with 0.575(3)/0.425(3) found in $Li_{16.42(1)}Si_4$. Analogously to $Li_{16.42(1)}Si_4$,[10] a split position for Li5 on 8*f* (0, *x*, *y*) was introduced. The split fractions converged to 0.75(4) for Li5A and 0.25(4) for Li5B (0.848(7)/0.152(7) in $Li_{16.42(1)}Si_4$;[10] refinement details and the geometric relevance of the atom split are given in the ESI†). In case of atoms being uninvolved in disorder, site occupancy factors were refined to values close to full occupancy and therefore those positions were constrained to full occupancy. Thus, the unit cell contains 65.54(7) Li atoms as a consequence of the disorder (65.70(3) in $Li_{16.42(1)}Si_4$[10]) and 16 Ge atoms, resulting in a crystallographic density of 2.011 g cm^{-3}. The structure was finally solved with reliability factors of R_1 = 0.023 and wR_2 = 0.027 for all data (Table 6). $Li_{16.38(2)}Ge_4$ crystallizes isotypically with $Li_{16.42(1)}Si_4$.[10]

Table 2 Fractional atomic coordinates and isotropic equivalent atomic displacement parameters for $Li_{4.096(4)}Ge$ (*Cmcm*, Z = 16, T = 100 K, estimated standard deviations in parentheses)

Atom	Wyckoff position	x	y	z	s.o.f.	$U_{eq.}$/Å^2·10^3
Ge1	4*c*	0	0.256372(6)	1/4	1	7.83(3)
Ge2	4*c*	1/2	0.454314(5)	1/4	1	6.35(3)
Ge3	8*f*	1/2	0.105220(4)	0.067609(6)	1	6.83(2)
Li1	4*c*	1/2	0.0333(1)	1/4	1	14.4(4)
Li2	4*c*	1/2	0.3297(1)	1/4	1	13.5(4)
Li3	4*c*	0	0.3922(1)	1/4	1	17.5(5)
Li4A	4*c*	1/2	0.1476(2)	1/4	0.616(8)	52(3)
Li4B	8*g*	0.210(1)	0.1385(2)	1/4	0.384(8)	21(2)
Li5A	8*f*	0	0.1741(3)	0.0842(7)	0.75(4)	14(1)
Li5B	8*f*	0	0.164(1)	0.123(4)	0.25(4)	24(6)
Li6	8*f*	0	0.04650(7)	0.1225(1)	1	13.9(3)
Li7	8*f*	0	0.31636(9)	0.0788(1)	1	16.5(3)
Li8	8*f*	0	0.47089(9)	0.0908(1)	1	18.7(3)
Li9	8*f*	1/2	0.23155(8)	0.1356(1)	1	19.1(3)
Li10	8*f*	1/2	0.40425(8)	0.0639(1)	1	14.5(3)

Structure description of $Li_{17}Ge_4$ and $Li_{16.38}Ge_4$

In our previous work we reported on the structures of $Li_{17}Si_4$ and $Li_{16.42}Si_4$ in detail.[9,10] Both phases were comparatively highlighted on the basis of $SiLi_n$ coordination polyhedra and the disorder in $Li_{16.42}Si_4$ was illustrated with various structure models. Hence, we analogously elaborate on the structures of the isotypic phases $Li_{17}Ge_4$ and $Li_{16.38}Ge_4$ herein.

The structure of $Li_{17}Ge_4$ is closely related to the previously reported phase $Li_{21}Ge_5$[24] ($Li_{16.8}Ge_4$) only differing in the occupation of one fourfold special position. In detail, their common space group $F\bar{4}3m$ possesses four positions with site symmetry $\bar{4}3m$ (4*a*–*d*). Whereas Wyckoff positions 4*a*–*d* were claimed to be void in $Li_{21}Ge_5$, we found a fully occupied 4*a* site in $Li_{17}Ge_4$ with short but reasonable next nearest neighbor distances of 2.397(7) Å for Li1–Li13 (*cf.* Fig. 3 and Table 4). We note that since $Li_{22}Si_5$[27,45] (its composition corresponds to a full occupancy of sites 4*a*–*d*) was revised to $Li_{21}Si_5$,[46] heavier analogues such as $Li_{22}Ge_5$ were supposed to crystallize with the $Li_{21}Si_5$ structure type as well ($Li_{21}Ge_5$).[24] We have already shown by computational methods that the fully relaxed structures of $Li_{17}Si_4$ and $Li_{21}Si_5$ decisively differ regarding the coordination environment around the 4*a* site.[9] If this position is unoccupied, the first coordination shell, which is a $(Li1)_4$ tetrahedron (*cf.* Fig. 3), is markedly contracted, which was not observed in experimental data of $Li_{21}Si_5$ (Table S5 in the ESI†). Therefore it could be concluded that Li might have been overseen in the previous structure refinement (most likely a partial occupancy). Turning to $Li_{17}Ge_4$, the positional parameters are almost identical with $Li_{17}Si_4$ (Table S6 in the ESI†) and therefore an equal conclusion is reasonable.

In 2001, Goward *et al.*[18] have already reported on the revision of $Li_{22}M_5$ to $Li_{17}M_4$ (M = Ge, Sn, Pb). However, their model for "$Li_{17}Ge_4$" involved partially occupied Li sites (Table 3), namely Li1A on 16*e* (3/4 occ.), Li1B on 16*e* (1/4 occ.), and Li13 on 4*a* (3/4 occ.) resulting in the composition $Li_{16.95}Ge_4$ (note that for a better comparability the fractional atomic coordinates and labels were adapted to $Li_{17}Ge_4$). In the case of a void 4*a* site, the surrounding $(Li1A)_4$ tetrahedron (comparable with Li1 in Fig. 3) is slightly contracted to $(Li1B)_4$ whose vertices are markedly closer to the 4*a* center (2.52 Å *vs.* 1.91 Å).[18] Interestingly, this scenario is in close agreement with the computationally relaxed structure of $Li_{21}Si_5$[9] (Table S7 in the ESI†) where all fourfold positions are void. Consequently, a partial occupancy of the 4*a* position as reported for $Li_{16.95}Ge_4$ and hence the existence of a small homogeneity

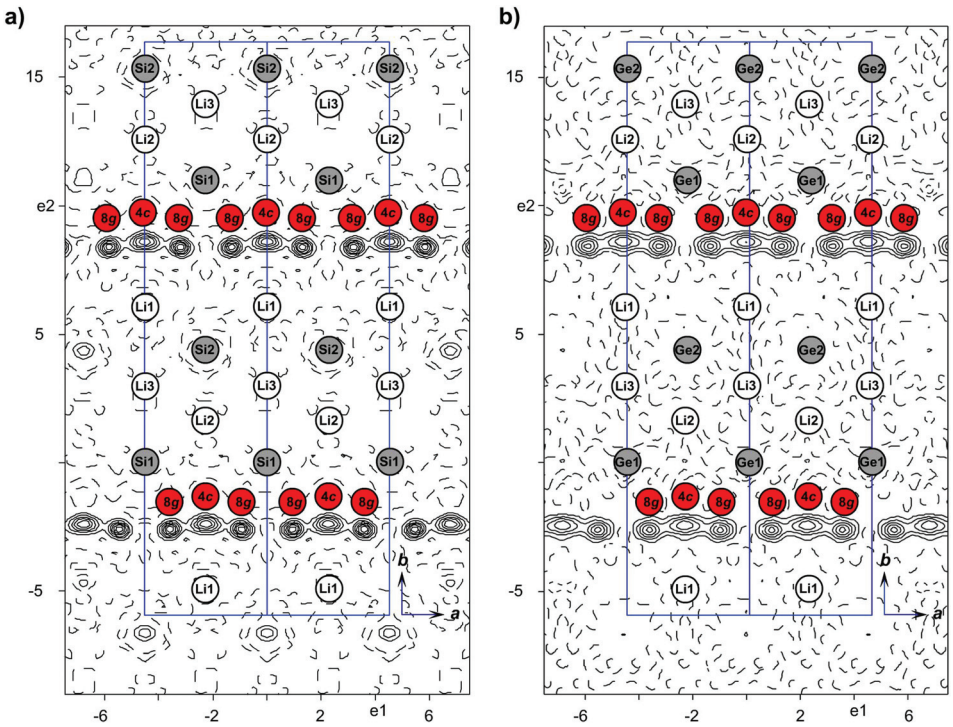

Fig. 2 Difference Fourier map ($F_o - F_c$) shown for the layer defined by Tt1, Tt2 and Li2 in (a) $Li_{16.42}Si_4$[10] and (b) $Li_{16.38}Ge_4$ (parallel to the *ab*-plane, calculated from single crystal data at 100 K and 123 K for $Li_{16.42}Si_4$ (contour lines ±0.6 e Å^{-3}) and $Li_{16.38}Ge_4$ (contour lines ±0.5 e Å^{-3}), respectively; cell edges are shown in blue).

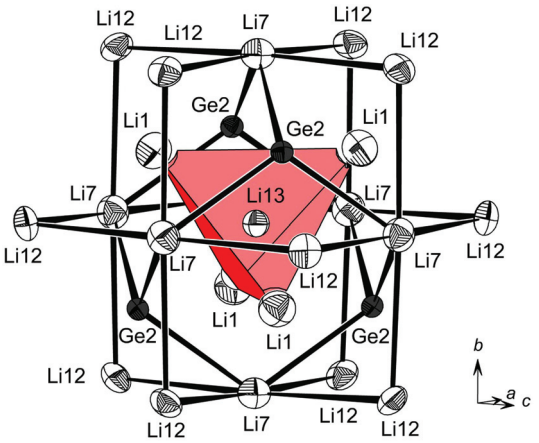

Fig. 3 Coordination environment of Li13 on the Wyckoff position 4*a* (Ge = black; Li = white; thermal ellipsoids at 70% probability, single crystal data at room temperature). The 1st, 2nd, 3rd, and 4th coordination shell is formed by a $(Li1)_4$ and $(Ge2)_4$ tetrahedron as well as a $(Li7)_6$ octahedron and a $(Li12)_{12}$ cuboctahedron.

region $Li_{17-x}Tt_4$ ($0 < x < 0.2$) are indeed meaningful. More recently, Lacroix-Orio *et al.*[47] presented a Zn-doped derivative of the $Li_{17}Ge_4$ compound. They could not find any evidence for partially occupied Li positions and instead found small concentrations of Zn being incorporated at the 4*a* position ($Li_{17-\varepsilon}Zn_\varepsilon Ge_4$, $\varepsilon = 0.005(1)$).

Concluding, the fractional atomic coordinates of all $Li_{17}Ge_4$ related phases listed in Table 3 are very similar and the scenario of an unoccupied 4*a* position in $Li_{16.95}Ge_4$ fits the calculated data of the corresponding $Li_{21}Si_5$ structure very well. This strengthens the existence of a homogeneity region $Li_{17-x}Tt_4$ ($0 < x < 0.2$) which is deduced from the flexibility of the $(Li1)_4(Tt_2)_4$ tetrahedral star around the Wyckoff position 4*a*.[9] Accordingly, the herein reported phase $Li_{17}Ge_4$ is regarded as the lithium-richest representative in the Li–Ge system.

The structure of $Li_{17}Ge_4$ is closely related to a 6 × 6 × 6 superstructure of the body centered cubic (bcc) structure.[46] As already shown by von Schnering and Nesper,[46] it can be easily interpreted by 26 atom clusters (M_{26} with M = Tt, Li) centered at the special positions 4*a*–*d* whereas Ge_4 tetrahedra and Ge_6 octahedra (note that Ge atoms are isolated by distances larger than 4.44 Å) are situated around 4*a*, 4*c* and 4*b*, 4*d*, respectively, corresponding to the arrangement of Na and Tl atoms in the NaTl structure.[46]

Yet another possible way of looking at the structure of $Li_{17}Ge_4$ is the comparison of $GeLi_n$ coordination polyhedra and their arrangement in the unit cell. This has proven to be a neat method for the comparison of lithium-rich Li–Si phases solely bearing isolated Si atoms in their structures ($Li_{17}Tt_4$, $Li_{16.4}Tt_4$ and $Li_{15}Tt_4$).[10] As shown in Fig. 4a, Ge1, Ge3 and Ge4 are 13-coordinated by Li atoms, whereas Ge2 attains a coordination number (CN) of 14. Corresponding to the first coordination shell of Ge atoms, Li–Ge distances range from 2.659(4) Å to 3.053(3) Å (Table 4). The second Li shell is clearly separated with distances larger than 4.2564(3) Å. Interestingly, the polyhedra around Wyckoff positions 4*a*, 4*c* and 4*b*, 4*d* either form

Table 3 Comparison of fractional atomic coordinates for $Li_{17}Ge_4$, $Li_{17-\varepsilon}Zn_\varepsilon Ge_4$, and $Li_{16.95}Ge_4$ (space group $F\bar{4}3$ m (for all phases), Z = 20, estimated standard deviations in parentheses). Listed are x values for the special positions 16*e* (x, x, x), 24*f* (x, 0, 0), 24*g* (x, 1/4, 1/4) and x, z pairs for 48*h* (x, x, z)

At.	Wyck. pos.	$Li_{17}Ge_4$	$Li_{17-\varepsilon}Zn_\varepsilon Ge_4$[47]	$Li_{16.95}Ge_4$[18]	At.	Wyck. pos.	$Li_{17}Ge_4$	$Li_{17-\varepsilon}Zn_\varepsilon Ge_4$[47]	$Li_{16.95}Ge_4$[18]
Ge1	16*e*	0.15955(1)	0.15958(2)	0.15952(5)	Li8	24*g*	0.0743(3)	0.0740(6)	0.075(1)
Ge2	16*e*	0.91657(1)	0.91667(3)	0.91684(5)	Li9	48*h*	0.0913(2)	0.0906(3)	0.0907(7)
Ge3	24*f*	0.32102(1)	0.32118(4)	0.32112(7)			0.2624(2)	0.2631(4)	0.2660(8)
Ge4	24*g*	0.57015(1)	0.57020(4)	0.56965(7)	Li10	48*h*	0.0896(2)	0.0904(4)	0.0914(7)
Li1A	16*e*	0.0734(2)	0.0747(6)	0.0775			0.7612(2)	0.7613(4)	0.7597(9)
Li1B	16*e*	—	—	0.0587	Li11	48*h*	0.1547(1)	0.1554(3)	0.1540(5)
Li2	16*e*	0.3031(2)	0.3033(3)	0.3032(6)			0.5205(2)	0.5216(4)	0.5216(9)
Li3	16*e*	0.4175(2)	0.4179(5)	0.4169(9)	Li12	48*h*	0.1637(1)	0.1632(3)	0.1625(5)
Li4	16*e*	0.5575(2)	0.5584(4)	0.5579(6)			0.0027(2)	0.0025(5)	0.005(1)
Li5	16*e*	0.6877(2)	0.6864(4)	0.6876(7)	Li13	4*a*	0	0	0
Li6	16*e*	0.8314(2)	0.8331(4)	0.8329(7)	Zn1	4*a*	—	0	—
Li7	24*f*	0.1677(3)	0.1678(6)	0.170(1)					

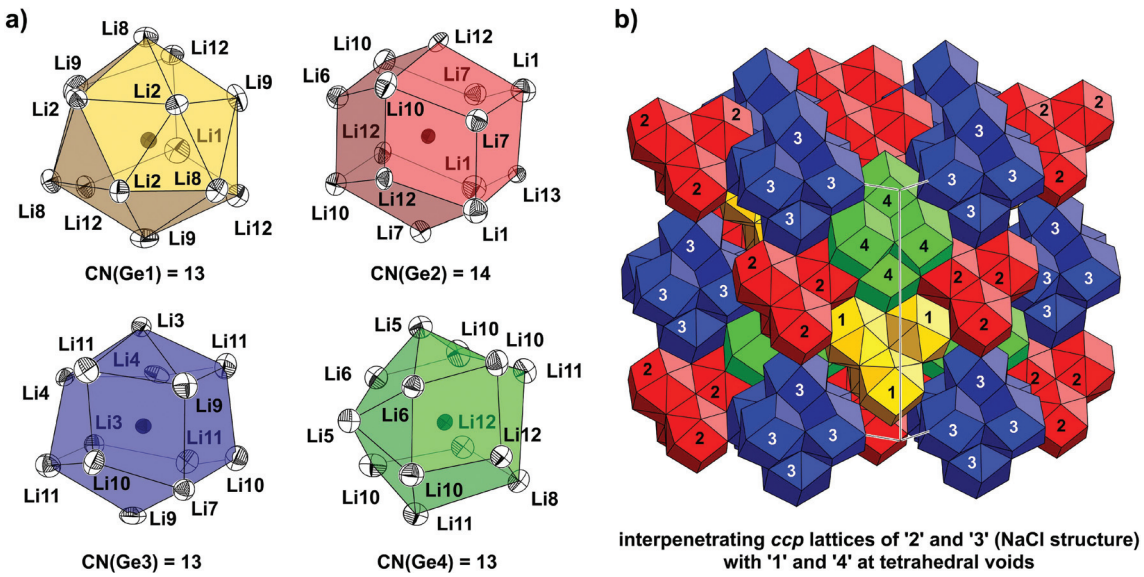

Fig. 4 (a) $GeLi_n$ coordination polyhedra (CN = coordination number) and (b) their relative arrangement in the cubic unit cell of $Li_{17}Ge_4$ (Ge = black; Li = white; thermal ellipsoids at 70% probability, single crystal data at room temperature). Supratetrahedra and supraoctahedra are formed from $Ge1Li_{13}$, $Ge2Li_{14}$ and $Ge3Li_{13}$, $Ge4Li_{13}$ coordination polyhedra (denoted as 1, 2, 3 and 4).

supratetrahedra ($[Ge1Li_{13}]_4$ and $[Ge2Li_{14}]_4$ denoted as (1) and (2)) or supraoctahedra ($[Ge3Li_{13}]_6$ and $[Ge4Li_{13}]_6$ denoted as (3) and (4)), respectively (Fig. 4b). Accordingly, the structure of $Li_{17}Ge_4$ can be considered as two interpenetrating *ccp* lattices of (2) and (3), *i.e.* the NaCl structure, where tetrahedral voids are filled with (1) and (4).

Besides $Li_{17}Ge_4$ and $Li_{15}Ge_4$, $Li_{16.38}Ge_4$ is yet another representative exclusively bearing isolated Ge atoms. It is isotypic with $Li_{16.42}Si_4$[10] which possesses a peculiar structure involving occupational and positional disorder along the crystallographic *a*-axes (*cf.* Fig. 2). A convenient way of illustrating the disordered structure of $Li_{16.38}Ge_4$ is the assumption of a simplified ordered model which has already been applied for the description and band structure calculations of $Li_{16.42}Si_4$.[10] In detail, the atom positions Li4A, Li4B and Li5A (*cf.* Table 2) affected by disorder corresponding to the Wyckoff positions 4*c*

Table 4 Selected interatomic distances in $Li_{17}Ge_4$ ($F\bar{4}3m$, Z = 20, T = 298 K, estimated standard deviations in parentheses)

Atom pair			*d*(Å)	Atom pair			*d*(Å)
Ge1	Li9	×3	2.659(4)	Ge3	Li10	×2	2.849(4)
	Li1		2.813(7)		Li3	×2	2.855(2)
	Li2	×3	2.884(1)		Li7		2.890(5)
	Li8	×3	2.898(3)		Li11	×4	2.977(2)
	Li12	×3	2.959(4)	Ge4	Li12	×2	2.680(3)
Ge2	Li12	×3	2.686(3)		Li11	×2	2.709(3)
	Li13		2.7244(3)		Li8		2.723(5)
	Li7	×3	2.734(3)		Li5	×2	2.769(4)
	Li6		2.780(6)		Li6	×2	2.856(2)
	Li10	×3	2.933(4)		Li10	×4	3.053(3)
	Li1	×3	2.969(4)	Li13	Li1	×4	2.397(7)
Ge3	Li9	×2	2.673(4)		Ge2	×4	2.7244(3)
	Li4	×2	2.760(3)		Li7	×6	3.162(5)

(0.616(8) occ.), 8*g* (0.384(8) occ.) and 8*f* (0.75(4) occ.), respectively, are either regarded as half (Li4A, Li4B) or fully occupied (Li5A) resulting in the composition $Li_{16.5}Ge_4$. An accordingly ordered model with fully occupied atom positions and crystallographically independent sites for Li4B′ and Li4B″ (translate to Li4B in *Cmcm*) can be achieved by symmetry reduction and a cell enlargement (space group $P2_1/m$, a = 9.1016(4) Å, b = 13.2751(4) Å, c = 11.2744(4) Å, β = 101.643(1)°; for crystallographic details, see ref. 10). The $GeLi_n$ polyhedra occurring in the respective model "$Li_{16.5}Ge_4$" are depicted in Fig. 5a.

Similar to $Li_{17}Ge_4$, the first shell of Li atoms surrounding each Ge atom is clearly separated from the second one with distances between 2.596(2) Å to 3.309(3) Å and distances above 4.103(4) Å (Table 5). Whereas Ge1 and Ge2 are permanently 13-coordinated ($Ge1Li_{13}$/$Ge1'Li_{13}$ and $Ge2Li_{13}$ denoted as (1)/(1′) and (2)), Ge3 attains coordination numbers of either 12 or 13 ($Ge3Li_{12}$ and $Ge3'Li_{13}$ denoted as (3) and (3′)). The different coordination of Ge3 is attributed to the varying occupation of atom positions Li4A, Li4B′ and Li4B″. The arrangement of $GeLi_n$ polyhedra in the unit cell of $Li_{16.38}Ge_4$ is achieved by stacking them into strands which proceed along the crystallographic *a*-axis (Fig. 5b). For the ordered model "$Li_{16.5}Ge_4$", the stacking sequence is indicated by numbers corresponding to various $GeLi_n$ polyhedra highlighted in Fig. 5a.

Comparing the $TtLi_n$ coordination polyhedra of all lithium-rich Li–Tt phases, which exclusively comprise isolated Tt atoms in their structures, the coordination numbers consistently increase from CN = 12 ($Li_{15}Tt_4$), over CN = 12–13 ($Li_{16.4}Tt_4$) to CN = 13–14 ($Li_{17}Ge_4$).

Solid solutions $Li_{17}Si_{4-x}Ge_x$ [x = 2.30(2), 3.08(4), 3.53(3)]

$Li_{17}Si_4$ and $Li_{17}Ge_4$ are isotypic phases that form solid solutions. Single crystalline samples of $Li_{17}Si_{4-x}Ge_x$ were obtained from melt equilibration experiments and analyzed by single crystal and powder X-ray diffraction as well as energy dispersive X-ray spectroscopy. The Si–Ge ratios for $Li_{17}Si_{4-x}Ge_x$ samples obtained from single crystal X-ray diffraction data were x = 2.30(2), 3.08(4), and 3.53(3). We note that these values deviate from the initial ones x = 1.0, 2.0, and 3.0 corresponding to the employed melts "$Li_{90}Si_{7.5}Ge_{2.5}$", "$Li_{90}Si_5Ge_5$" and "$Li_{90}Si_{2.5}Ge_{7.5}$" as the Si amount is reduced due to a partial reaction of Si with the stainless steel ampules; thus the Si–Ge ratios in the products are shifted toward higher Ge contents. As can be seen in Fig. 6, the cell axes and volumes (determined from PXRD patterns of the respective samples by Rietveld refinement, Fig. S2†) linearly increase with increasing Ge concentrations in $Li_{17}Si_{4-x}Ge_x$ revealing a perfect behavior obeying Vegard's law.[43] Additionally, results from EDX measurements agree well with the crystallographically determined Si–Ge ratios (impurities originating from the stainless steel ampule were not detected).

Analyzing the distribution of Si and Ge on atom positions Tt1–4, the Si–Ge ratios are very similar for Tt1, Tt3, and Tt4, whereas Tt2 on the Wyckoff position 16*e* (x, x, x) features a slight preference for Si (Table S1–4†). Comparing the coordination environment of Tt2 and Tt1, Tt3, Tt4, the former is

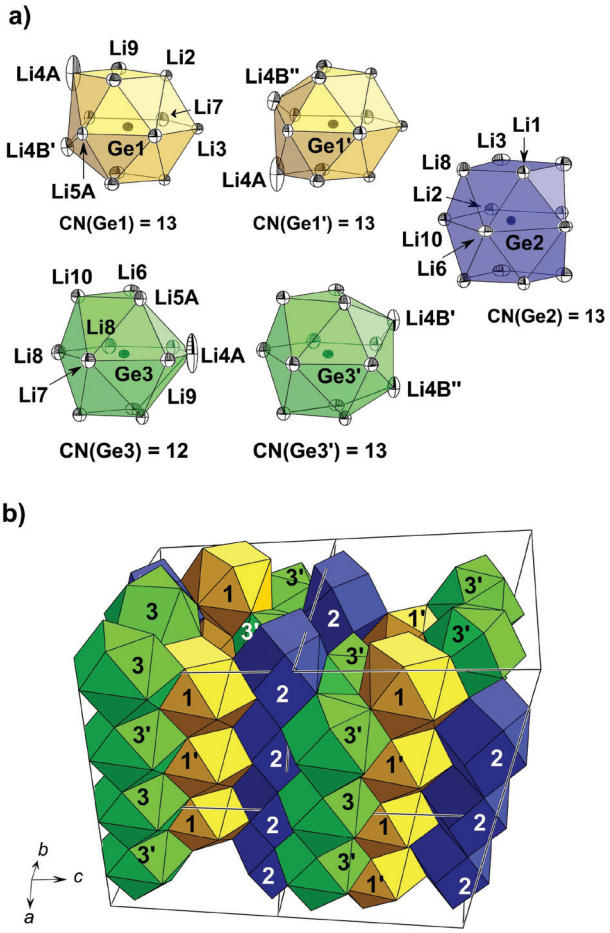

Fig. 5 (a) $GeLi_n$ coordination polyhedra occurring in an idealized model for $Li_{16.38}Ge_4$ with a composition of $Li_{16.5}Ge_4$ (space group $P2_1/m$, fully occupied and crystallographically independent atom positions Li4B′, Li4B″ (both correspond to Li4B in $Li_{16.38}Ge_4$), Li4A, and Li5A); (b) stacking of $GeLi_n$ polyhedra by sharing opposite faces resulting in parallel rods which run along the crystallographic *a*-axis (Ge = black, Li = white, thermal ellipsoids at 90% probability, single crystal data at 100 K). The polyhedra stacking in the structure model "$Li_{16.5}Ge_4$" is indicated by numbers *X* which correspond to the coordination polyhedra of atom Ge*X* in (a).

Table 5 Selected interatomic distances in $Li_{16.38}Ge_4$ (*Cmcm*, Z = 16, T = 123 K, estimated standard deviations in parentheses)

Atom pair			d(Å)	Atom pair			d(Å)
Ge1	Li7	×2	2.631(2)	Ge2	Li8	×4	3.127(1)
	Li5B	×2	2.64(2)	Ge3	Li4A		2.596(2)
	Li4B	×2	2.772(4)		Li7		2.603(2)
	Li9	×4	2.790(1)		Li8		2.693(2)
	Li2	×2	2.792(1)		Li6	×2	2.7188(9)
	Li5A	×2	2.854(8)		Li5B	×2	2.723(8)
	Li3		3.001(2)		Li5A	×2	2.747(3)
	Li4A	×2	3.309(3)		Li4B	×2	2.854(3)
Ge2	Li6	×2	2.647(2)		Li10	×2	2.875(1)
	Li3	×2	2.657(1)		Li1		2.896(1)
	Li10	×2	2.707(2)		Li9		2.932(2)
	Li2		2.753(2)		Li8		2.983(2)
	Li1	×2	2.867(2)				

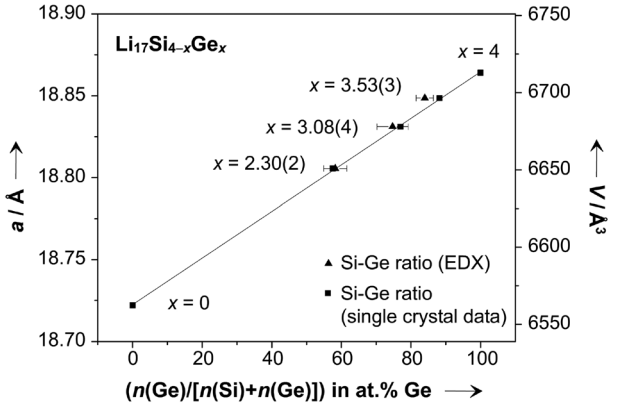

Fig. 6 Trend of cell volumes *vs.* Ge contents in $Li_{17}Si_{4-x}Ge_x$ (x = 0, 2.30(2), 3.08(4), 3.53(3), 4). Cell parameters were determined from respective PXRD patterns by Rietveld refinement (Fig. S2), and Ge contents were obtained from either single crystal X-ray diffraction data or EDX (error bars for a, V, and $x_{single\ crystal}$ (in at%) are smaller than data point icons).

14- and the latter are 13-coordinated by Li atoms with similar Ge–Li distances (2.68 Å–2.95 Å *vs.* 2.65–3.04 Å). The phenomenon that different crystallographic sites are substituted differently is also known as the "coloring problem".[48] In some cases the site preferences cannot be deduced on the basis of simple chemical reasoning (*e.g.* differences in electronegativities) and quantum chemical calculations may give a reasonable explanation.[49] Here, the focus is set on experimental work and we note that small differences in the distribution of Si and Ge on atom positions Tt2 and Tt1, Tt3, Tt4 were traced.

Thermodynamic stability of $Li_{17}Ge_4$ and $Li_{16.38}Ge_4$

The Li–Ge phase diagram was determined by Federov & Molochka[23] in 1966 and later revised by Grüttner[25] in his dissertation. However, a current compilation of the Li–Ge system[50] did not include Grüttner's results and, hence, significant information is missing. Therefore and due to the recent improvements of the Li–Si phase diagram (>76 at% Li),[8–10] a detailed redetermination of the respective portion of the Li–Ge system is essential.

The lithium-rich section of the Li–Ge phase diagram (>79 at % Li) was studied by DSC investigations of samples with systematically different compositions $Li_{17}Ge_4$, "$Li_{16.5}Ge_4$" and "$Li_{16}Ge_4$". Accordingly, PXRD patterns correspond to pure-phase $Li_{17}Ge_4$, a mixture of $Li_{17}Ge_4$ and $Li_{16.38}Ge_4$, and a mixture of $Li_{16.38}Ge_4$ and $Li_{15}Ge_4$, respectively (Fig. 7).

The thermograms of these samples are depicted in Fig. 7. The first thermal events in these cooling traces (signal 1–3) are assigned to the crossing of the liquidus boundary. Analogously to the Li–Si system,[10] signals (4) and (5) at 520–522 °C and 627 °C are attributed to the peritectic formation temperatures of $Li_{17}Ge_4$ (481–486 °C for $Li_{17}Si_4$) and $Li_{16.38}Ge_4$ (618 °C for $Li_{16.42}Si_4$), respectively. This is additionally strengthened by our results from melt equilibration experiments (see above) where crystals of $Li_{16.38}Ge_4$ are only afforded above temperatures of 520 °C. Note that signal (5) corresponding to the peritectic formation of $Li_{16.38}Ge_4$ from melt and $Li_{15}Ge_4$ is superimposed by signals (1) and (2) in the cooling traces of $Li_{17}Ge_4$ and "$Li_{16.5}Ge_4$" (Fig. 7), respectively, but clearly visible for the "$Li_{16}Ge_4$" sample. Instead, it can be recognized at around 630 °C in the respective heating trace, exemplarily shown for $Li_{17}Ge_4$ (effect 5′). Furthermore, long term annealing experiments of "$Li_{16}Ge_4$" samples (Fig. S1 in the ESI†) established $Li_{16.38}Ge_4$ as a high-temperature phase being stable above ~400 °C until 627 °C, just like $Li_{16.42}Si_4$ existing between 470 and 618 °C.[10] We note that the decomposition behavior of $Li_{16.38}Ge_4$ is very sluggish and even harder to trace than in the case of its Si counterpart.

Finally, the recent results from DSC investigations are compiled in an updated Li–Ge phase diagram (Fig. 8b) which was revised from Grüttner's previously determined one shown in Fig. 8a. A comparison with the Li–Si phase diagram (Fig. 8c) reveals similarities to the Li–Ge system. An interesting difference is the stability of $Li_{15}Tt_4$. Whereas $Li_{15}Si_4$ is metastable and decomposes above ~170 °C,[8] $Li_{15}Ge_4$ is thermodynamically stable and melts congruently at 720 °C.[25] Furthermore, uncertainties regarding the isotherms at 610 °C and 618 °C in the Li–Si phase diagram[10] could not be found for the Li–Ge system.

Conclusion

The germanides $Li_{17}Ge_4$ and $Li_{16.38}Ge_4$ were established as further representatives of the Li–Ge system. The latter is assigned a high-temperature phase which exists between ~400 and 627 °C, the former, the lithium-richest Li–Ge phase, decomposes peritectically at 521 °C into melt and $Li_{16.38}Ge_4$. $Li_{16.38}Ge_4$ can be retained at room temperature if according melts are cooled to the respective temperature region and subsequently quenched. Both germanides are isotypic to the silicides $Li_{17}Si_4$ and $Li_{16.42}Si_4$ extending the family of isotypic lithium tetrelides to $Li_{17}Tt_4$, $Li_{16.4}Tt_4$, $Li_{15}Tt_4$, $Li_{14}Tt_6$, $Li_{12}Tt_7$, and LiTt (Tt = Si, Ge). The previously reported $Li_{16.95}Ge_4$ can be regarded as representative of a homogeneity region $Li_{17-x}Tt_4$ ($0 < x < 0.2$) with $Li_{17}Ge_4$ and $Li_{16.8}Ge_4$ ($Li_{21}Ge_5$) as border phases only differing in the occupation of the Wyckoff position 4*a*. Moreover, the validity of Vegard's law for the solid solutions $Li_{17}Si_{4-x}Ge_x$ was confirmed and small differences in the distribution of Si and Ge to the four crystallographically independent atom positions were observed. Regarding the thermodynamic properties, the regions of stability for $Li_{17}Tt_4$ and $Li_{16.42}Tt_4$ are very similar. Interesting are also the thermodynamic and structural differences of lithium silicides and germanides. For instance, whereas $Li_{15}Si_4$ is a metastable phase, $Li_{15}Ge_4$ melts congruently at 720 °C. Further, the phases Li_9Ge_4 and Li_7Ge_{12} are not known in the Li–Si system. In particular, the synthesis of a hypothetical phase Li_7Si_{12} would be an intriguing field of research since it may serve as a precursor for a new allotrope of Si, just as was reported for Li_7Ge_{12} and its mild oxidation to *allo*-Ge.[36,51]

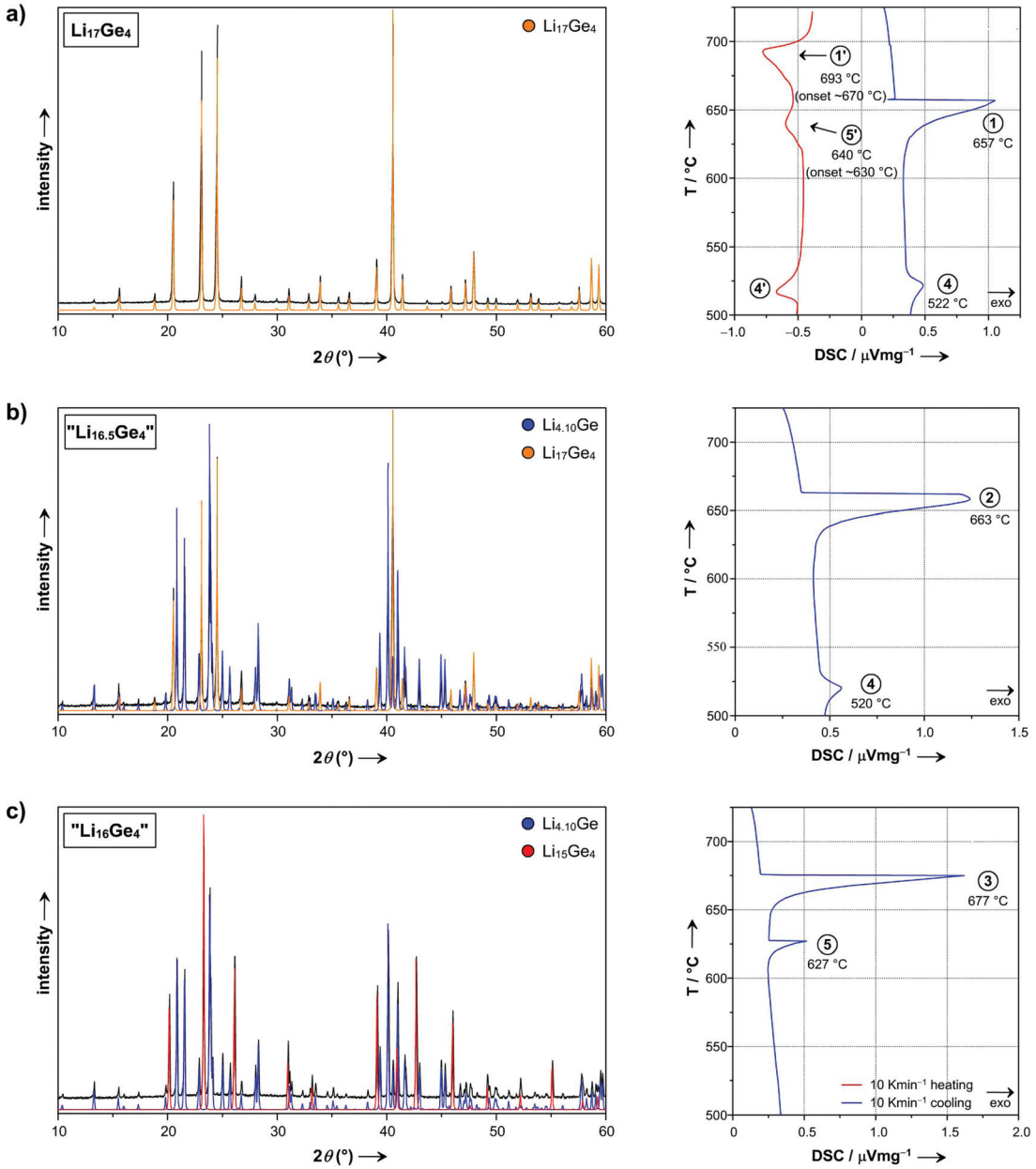

Fig. 7 PXRD patterns and corresponding DSC thermograms of bulk samples (a) $Li_{17}Ge_4$, (b) $Li_{16.5}Ge_4$, and (c) $Li_{16}Ge_4$ (PXRD patterns: experimental = black, $Li_{17}Ge_4$ (calc.) = yellow, $Li_{4.10}Ge$ (calc.) = blue, $Li_{15}Ge_4$ (calc.) = red; DSC thermograms: heating and cooling traces are shown in red and blue, respectively, a signal assignment is given in the Li–Ge phase diagram in Fig. 8b).

Experimental section

Synthesis

Starting materials were Li rods (99%, Rockwood-Lithium), Si powder (99.999%, Alfa Aesar) and Ge pieces (99.999%, Chempur). All steps of synthesis and sample preparation were carried out in a glove box (MBraun, Ar atmosphere, H_2O and O_2 levels <0.1 ppm). Ta and stainless steel ampules were thoroughly cleaned, heated to 1000 °C (Ta) or 800 °C (stainless steel) under dynamic vacuum ($p < 1 \times 10^{-3}$ mbar) for at least 2 h and transferred to the glove box. An all-glass Schlenk line supplied with Ar, which is dried over P_2O_5, molecular sieve and heated titanium sponge (T = 750 °C), was used for heating and handling under inert conditions.

Large single crystals of $Li_{17}Ge_4$ and $Li_{4.10}Ge$ ($Li_{16.38}Ge_4$) (*cf.* Fig. 1) were obtained from equilibrating melts with compositions "$Li_{95}Ge_5$" and "$Li_{85}Ge_{15}$" at temperatures of 400 and 530 °C in Ta ampules (slow cooling from 700 °C at a rate of 5 K h^{-1} followed by 48 hours dwelling at specified temperatures) and subsequent isothermal melt-centrifugation. Details of this procedure have already been described in ref. 9 and 52. Crystals of $Li_{17}Si_{4-x}Ge_x$ [x = 0, 2.30(2), 3.08(4), 3.53(3)] were

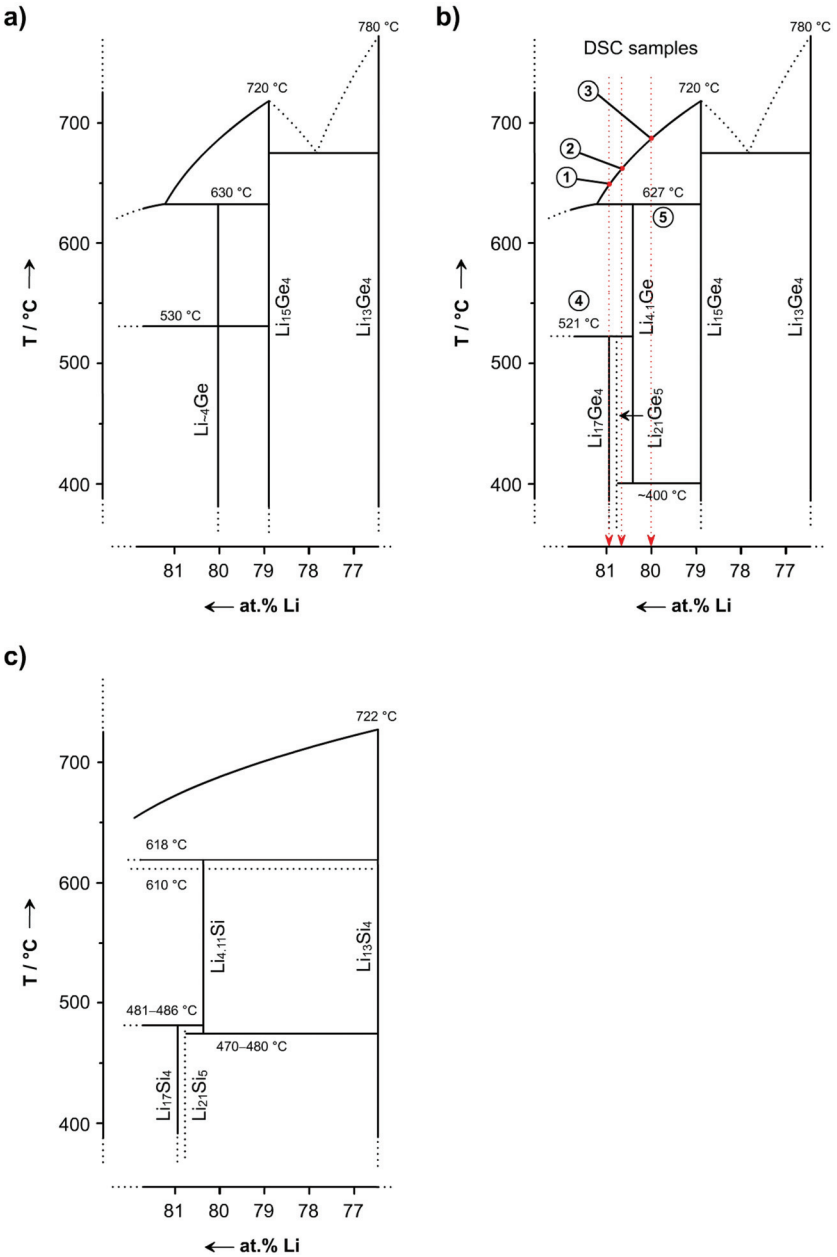

Fig. 8 (a) Excerpt of the Li–Ge phase diagram as reported from Grüttner[25] (the composition of the eutectic between $Li_{15}Ge_4$ and $Li_{13}Ge_4$ was not determined), (b) its revision based on DSC investigations and annealing experiments of "$Li_{16}Ge_4$" samples reported herein, and (c) the most recent Li–Si phase diagram for Li concentrations >76%.[10]

grown analogously in stainless steel ampules from melts with compositions "$Li_{90}Si_{10}$", "$Li_{90}Si_{7.5}Ge_{2.5}$", "$Li_{90}Si_5Ge_5$" and "$Li_{90}Si_{2.5}Ge_{7.5}$" equilibrated at 450 °C.

Furthermore, elemental mixtures with compositions $Li_{17}Ge_4$, "$Li_{16.5}Ge_4$" and "$Li_{16}Ge_4$" with a total amount of 2.5 g each were loaded into Ta ampules which were sealed by arc welding inside the glove box. For achieving targeted compositions with sufficient precision, a batch size of 2.5 g was deemed appropriate to keep weighing errors minimal.[9,10] Subsequently, ampules were sealed in silica jackets under vacuum and annealed in a muffle furnace. The temperature was raised to 750 °C at a rate of 10 K min^{-1} and held for 0.5 h followed by cooling to 500–550 °C at a rate of 10 K min^{-1}. After a dwell time of one hour, ampules were quenched in water and transferred back to the glove box. Obtained products were ground in agate mortars and characterized by powder X-ray diffraction (*cf.* Fig. 7).

Differential scanning calorimetry (DSC)

Differential scanning calorimetry was carried out with a Netzsch DSC 404 Pegasus apparatus. Cylindrical Nb crucibles (L = 15.0 mm, OD = 6.5 mm, ID = 5.0 mm) were thoroughly

cleaned, heated to 1000 °C under dynamic vacuum ($p < 1 \times 10^{-3}$ mbar) for 2 h and transferred to an Ar-filled glove box. Crucibles were loaded with 30–50 mg of the sample ($Li_{17}Ge_4$, "$Li_{16.5}Ge_4$" and "$Li_{16}Ge_4$"). Subsequently, the open end was roughly closed by crimping and then sealed by arc-welding inside the glove box under cooling. A sealed Nb crucible without the sample served as a reference. For all measurements an Ar-flow of 60–70 mL min^{-1} and a heating/cooling rate of 10 K min^{-1} were used. Samples were recovered after the measurement inside an Ar-filled glove box. Data were handled with the program Proteus Thermal Analysis.[53]

Annealing experiments

In order to further investigate the thermodynamic stability of $Li_{4.10}Ge$ ($Li_{16.38}Ge_4$), batches of 100–150 mg of "$Li_{16}Ge_4$" bulk material were sealed in Ta ampules and annealed in a muffle furnace at 200, 400 and 510 °C (10 K min^{-1} heating rate) for three days. Thereafter, ampules were quenched in water and transferred inside an Ar-filled glove box. Products were ground in agate mortars and subsequently characterized by powder X-ray diffraction (Fig. S1†).

Single crystal X-ray diffraction and structure determination

Crystals of $Li_{17}Ge_4$ and $Li_{4.096(4)}Ge$ ($Li_{16.38(2)}Ge_4$) were handled in an Ar-filled glove box, selected under a microscope and sealed inside glass capillaries. For the best specimen, intensity data were collected at room temperature ($Li_{17}Ge_4$) and 123 K ($Li_{16.38(2)}Ge_4$) on a Bruker X-ray diffractometer equipped with a CCD detector (Apex II, κ-CCD), a fine-focused sealed tube with MoK_α radiation (λ = 0.71073 Å) and a graphite monochromator using the Bruker Apex2 software.[54] Integration, data reduction and absorption correction were done using SAINT and SADABS.[55,56] The space groups $F\bar{4}3m$ ($Li_{17}Ge_4$) and *Cmcm* ($Li_{16.38(2)}Ge_4$) were assigned on the basis of the systematic absence and the statistical analysis of the intensity distributions. For $Li_{17}Ge_4$, Friedel pairs were not merged since the assigned space group is non-centrosymmetric. The Flack[57] parameter was determined as 0.50(3). The structures were solved by direct methods (Shelxs-97[58]) and refined with full-matrix least squares on F^2 (Shelxl-97[59]). Difference Fourier maps $F_o - F_c$ were calculated with Jana2006.[60] All refinement results are compiled in Table 6.

Details of the single crystal X-ray structure determination, refinement data, fractional atomic coordinates and isotropic equivalent atomic displacement parameters for $Li_{17}Si_{4-x}Ge_x$ [(x = 2.30(2), 3.08(4), 3.53(3)] are given in Table S1–4 in the ESI.† Further data may be obtained from Fachinformationszentrum Karlsruhe, D-76344 Eggenstein-Leopoldshafen, Germany (fax: (+49)7247-808-666; e-mail: crysdata@fiz-karlsruhe.de) on quoting the depository numbers CSD-427231 ($Li_{4.10}Ge$ ($Li_{16.38}Ge_4$)), CSD-427232 ($Li_{17}Ge_4$), CSD-427233 ($Li_{17}Si_{0.47}Ge_{3.53}$), CSD-427234 ($Li_{17}Si_{0.92}Ge_{3.08}$), and CSD-427235 ($Li_{17}Si_{1.70}Ge_{2.30}$).

Powder X-ray diffraction (PXRD)

PXRD patterns were recorded on a Stoe Stadi P diffractometer (Ge(111) monochromator for Cu$K_{\alpha1}$ radiation, λ = 1.54056 Å) equipped with a Dectris Mythen DCS 1 K solid state detector. Investigated samples were (i) single crystals of $Li_{17}Si_{4-x}Ge_x$ (x = 0, 2.30(2), 3.08(4), 3.53(3), 4), (ii) bulk samples of $Li_{17}Ge_4$, "$Li_{16.5}Ge_4$" and "$Li_{16}Ge_4$", and (iii) samples of "$Li_{16}Ge_4$" annealed at different temperatures. These were thoroughly ground in agate mortars, sealed inside 0.3 mm glass capillaries and measured in a 2θ-range of 5–90° (PSD steps: 0.06–1.00°; time per step: 20–40 s).

Table 6 Crystallographic data and structure refinement for $Li_{17}Ge_4$ and $Li_{4.096(4)}Ge$

Empirical formula	$Li_{17}Ge_4$	$Li_{4.096(4)}Ge$
T/K	298(2)	123(2)
Formula weight/g·mol^{-1}	408.34	101.01
Crystal size/mm^3	0.40 × 0.40 × 0.35	0.37 × 0.24 × 0.23
Crystal color	Metallic silver	Metallic silver
Crystal shape	Block	Bar
Space group	$F\bar{4}3m$	*Cmcm*
Structure type	$Li_{17}Pb_4$	$Li_{4.11}Si$
Unit cell dimension/Å	a = 18.8521(3)	a = 4.5511(2)
		b = 22.0862(7)
		c = 13.2751(4)
V/Å^3	6700.1(2)	1334.37(8)
Z	20	16
ρ (calc.)/g cm^{-3}	2.024	2.011
μ/mm^{-1}	8.832	8.860
F (000)	3580	709
θ Range/°	1.87–45.26	1.84–40.25
Index range hkl	$-37 \le h \le +23$	$-6 \le h \le +8$
	$-37 \le k \le +30$	$-32 \le k \le +40$
	$-37 \le l \le +37$	$-24 \le l \le +19$
Reflections collected	67 542	15 241
Independent reflections	2757 (R_{int} = 0.047)	2369 (R_{int} = 0.023)
Reflections with $I > 2\sigma(I)$	2547 (R_σ = 0.017)	1920 (R_σ = 0.017)
Data/restraints/parameter	2757/0/68	2369/0/82
Absorption correction	Multi-scan	Multi-scan
Goodness-of-fit on F^2	1.106	1.042
Final R indices $[I > 2\sigma(I)]^{a,b}$	R_1 = 0.018	R_1 = 0.015
	wR_2 = 0.037	wR_2 = 0.026
R indices (all data)^{a,b}	R_1 = 0.022	R_1 = 0.023
	wR_2 = 0.038	wR_2 = 0.027
Extinction coefficient	1.59(9) × 10^{-4}	1.52(7) × 10^{-3}
Flack parameter	0.50(3)	—
Largest diff. peak and hole/e Å^{-3}	0.46 and −0.69	0.69 and −0.52

$^a R_1 = \sum||F_o|-|F_c||/\sum|F_o|$. ^{b} w$R_2 = [\sum w(F_o^2 - F_c^2)^2/\sum w(F_o^2)^2]^{1/2}$.

Energy dispersive X-ray spectroscopy (EDX)

A Jeol-JSM 7500F scanning electron microscope equipped with an Oxford X-Max EDX analyzer with Mn as an internal standard was used for determining the Si–Ge ratios in $Li_{17}Si_{4-x}Ge_x$ [x = 2.30(2), 3.08(4), 3.53(3)]. Samples were handled inside an Ar-filled glove box and fixed on a graphite platelet which was mounted on an aluminum stub.

Acknowledgements

M.Z. thanks the Fonds der Chemischen Industrie for his fellowship, the authors thank K. Rodewald for EDX measurements.

References

1 M. N. Obrovac and L. Christensen, *Electrochem. Solid-State Lett.*, 2004, **7**, A93–A96.
2 T. D. Hatchard and J. R. Dahn, *J. Electrochem. Soc.*, 2004, **151**, A838–A842.
3 W. J. Zhang, *J. Power Sources*, 2011, **196**, 13–24.
4 P. Limthongkul, Y. I. Jang, N. J. Dudney and Y. M. Chiang, *Acta Mater.*, 2003, **51**, 1103–1113.
5 P. Limthongkul, Y. I. Jang, N. J. Dudney and Y. M. Chiang, *J. Power Sources*, 2003, **119–121**, 604–609.
6 B. Key, M. Morcrette, J. M. Tarascon and C. P. Grey, *J. Am. Chem. Soc.*, 2011, **133**, 503–512.
7 B. Key, R. Bhattacharyya, M. Morcrette, V. Seznec, J. M. Tarascon and C. P. Grey, *J. Am. Chem. Soc.*, 2009, **131**, 9239–9249.
8 M. Zeilinger, V. Baran, L. van Wüllen, U. Häussermann and T. F. Fässler, *Chem. Mater.*, 2013, **25**, 4113–4121.
9 M. Zeilinger, D. Benson, U. Häussermann and T. F. Fässler, *Chem. Mater.*, 2013, **25**, 1960–1967.
10 M. Zeilinger, I. M. Kurylyshyn, U. Häussermann and T. F. Fässler, *Chem. Mater.*, 2013, **25**, 4623–4632.
11 M. Zeilinger and T. F. Fässler, *Acta Crystallogr., Sect. E: Struct. Rep. Online*, 2013, **69**, i81–i82.
12 D. Thomas, M. Abdel-Hafiez, T. Gruber, R. Hüttl, J. Seidel, A. U. B. Wolter, B. Büchner, J. Kortus and F. Mertens, *J. Chem. Thermodyn.*, 2013, **64**, 205–225.
13 P. Wang, A. Kozlov, D. Thomas, F. Mertens and R. Schmid-Fetzer, *Intermetallics*, 2013, **42**, 137–145.
14 A. Debski, W. Gasior and A. Goral, *Intermetallics*, 2012, **26**, 157–161.
15 S. Dupke, T. Langer, R. Pöttgen, M. Winter, S. Passerini and H. Eckert, *Phys. Chem. Chem. Phys.*, 2012, **14**, 6496–6508.
16 S. Dupke, T. Langer, R. Pöttgen, M. Winter and H. Eckert, *Solid State Nucl. Magn. Reson.*, 2012, **42**, 17–25.
17 A. Kuhn, P. Sreeraj, R. Pöttgen, H. D. Wiemhöfer, M. Wilkening and P. Heitjans, *J. Am. Chem. Soc.*, 2011, **133**, 11018–11021.
18 G. R. Goward, N. J. Taylor, D. C. S. Souza and L. F. Nazar, *J. Alloys Compd.*, 2001, **329**, 82–91.
19 C. S. Fuller and J. C. Severiens, *Phys. Rev.*, 1954, **96**, 21–24.
20 J. Graetz, C. C. Ahn, R. Yazami and B. Fultz, *J. Electrochem. Soc.*, 2004, **151**, A698–A702.
21 E. M. Pell, *J. Phys. Chem. Solids*, 1957, **3**, 74–76.
22 G. I. Oleksiv, *Probl. Rozvitku Prirodn. i Tochn. Nauk, Sb.*, 1964, 76–77.
23 P. I. Federov and V. A. Molochka, *Izv. Akad. Nauk. SSSR, Neorg. Mater.*, 1966, **2**, 1870–1871.
24 R. Nesper, *Prog. Solid State Chem.*, 1990, **20**, 1–45.
25 A. Grüttner, PhD thesis, University of Stuttgart, 1982.
26 A. Grüttner, R. Nesper and H. G. von Schnering, *Acta Crystallogr., Sect. A: Cryst. Phys., Diffr., Theor. Gen. Cryst.*, 1981, **37**, C161.
27 E. I. Gladyshevskii, G. I. Oleksiv and P. I. Kripyakevich, *Kristallografiya*, 1964, **9**, 338–341.
28 Q. Johnson, G. S. Smith and D. Wood, *Acta Crystallogr.*, 1965, **18**, 131–132.
29 E. I. Gladyshevskii and P. I. Kripyakevich, *Kristallografiya*, 1960, **5**, 574–576.
30 R. Nesper, *Habilitation*, University of Stuttgart, 1988.
31 V. Hopf, W. Müller and H. Schäfer, *Z. Naturforsch., B: Anorg. Chem. Org. Chem.*, 1972, **27**, 1157–1160.
32 V. Hopf, H. Schäfer and A. Weiss, *Z. Naturforsch., B: Anorg. Chem. Org. Chem.*, 1970, **25**, 653.
33 H. G. von Schnering, R. Nesper, J. Curda and K. F. Tebbe, *Angew. Chem.*, 1980, **92**, 1070.
34 E. Menges, V. Hopf, H. Schäfer and A. Weiss, *Z. Naturforsch., B: Anorg. Chem. Org. Chem.*, 1969, **21**, 1351–1352. According to ref. 25, the structures of LiGe reported in ref. 22 and 34 are identical (only two different cell settings).
35 J. Evers, G. Oehlinger, G. Sextl and H. O. Becker, *Angew. Chem., Int. Ed. Engl.*, 1987, **26**, 76–78.
36 A. Grüttner, R. Nesper and H. G. von Schnering, *Angew. Chem., Int. Ed. Engl.*, 1982, **21**, 912–913.
37 U. Frank and W. Müller, *Z. Naturforsch., B: Anorg. Chem. Org. Chem.*, 1975, **30**, 313–315.
38 R. Nesper, J. Curda and H. G. von Schnering, *J. Solid State Chem.*, 1986, **62**, 199–206.
39 J. Evers, G. Oehlinger and G. Sextl, *Angew. Chem., Int. Ed. Engl.*, 1993, **32**, 1442–1444.
40 J. Evers and G. Oehlinger, *Angew. Chem., Int. Ed.*, 2001, **40**, 1050–1053.
41 F. Kiefer and T. F. Fässler, *Solid State Sci.*, 2011, **13**, 636–640.
42 Y. Hashimoto, N. Machida and T. Shigematsu, *Solid State Ionics*, 2004, **175**, 177–180.
43 L. Vegard, *Z. Phys.*, 1921, **5**, 17–26.
44 C. Lupu, J. G. Mao, J. W. Rabalais, A. M. Guloy and J. W. Richardson, *Inorg. Chem.*, 2003, **42**, 3765–3771.
45 H. Axel, H. Schäfer and A. Weiss, *Z. Naturforsch., B: Anorg. Chem. Org. Chem.*, 1966, **21**, 115–117.
46 R. Nesper and H. G. von Schnering, *J. Solid State Chem.*, 1987, **70**, 48–57.
47 L. Lacroix-Orio, M. Tillard and C. Belin, *J. Alloys Compd.*, 2008, **465**, 47–50.
48 G. J. Miller, *Eur. J. Inorg. Chem.*, 1998, 523–536.
49 N. Kazem, W. Xie, S. Ohno, A. Zevalkink, G. J. Miller, G. J. Snyder and S. M. Kauzlarich, *Chem. Mater.*, 2014, **26**, 1393–1403.
50 J. Sangster and A. D. Pelton, *J. Phase Equilib.*, 1997, **18**, 289–294 and references therein.
51 F. Kiefer, A. J. Karttunen, M. Döblinger and T. F. Fässler, *Chem. Mater.*, 2011, **23**, 4578–4586.
52 K. Puhakainen, M. Boström, T. L. Groy and U. Häussermann, *J. Solid State Chem.*, 2010, **183**, 2528–2533.
53 Netzsch Proteus Thermal Analysis, *Version 4.8.2*, Netzsch-Gerätebau GmbH, Selb, Germany, 2006.
54 APEX suite of crystallographic software, *APEX 2 Version 2008.4*, Bruker AXS Inc., Madison, WI, USA, 2008.
55 SAINT, *Version 7.56a*, Bruker AXS Inc., Madison, WI, USA, 2008.

56 SADABS, *Version 2008/1*, Bruker AXS Inc., Madison, WI, USA, 2008.
57 H. D. Flack, *Acta Crystallogr., Sect. A: Fundam. Crystallogr.*, 1983, **39**, 876.
58 G. M. Sheldrick, *Shelxs-97 – Program for the Determination of Crystal Structures*, University of Göttingen, Göttingen, Germany, 1997.
59 G. M. Sheldrick, *Shelxl-97 – Program for Crystal Structure Refinement*, University of Göttingen, Göttingen, Germany, 1997.
60 V. Petricek, M. Dusek and L. Palatinus, *Jana 2006: The Crystallographic Computing System, Version 03/15/2013*, Institute of Physics, Praha, Czech Rupublic, 2006.